# EXPERIMENTAL CHARACTERIZATION AND CONSTITUTIVE MODELLING OF TRANSPARENT POLYURETHANE

**Zisheng Liao[1], *Mokarram Hossain[2] and Xiaohu Yao[1]**

[1] School of Civil Engineering and Transportation, South China University of Technology, China
[2]Zienkiewicz Centre for Computational Engineering (ZCCE), Swansea University, UK

*mokarram.hossain@swansea.ac.uk

## Summary

Transparent polyurethane has been widely applied in laminated windshield glasses as the interlayer material to enhance the reliability due to its outstanding impact resistance. Under impact loading such as bird strike, the interlayer undergoes large tensile deformation at wide range of strain rates. In addition, the interlayer is on service over a wide range of temperatures for a plane traveling around the world. The mechanical behavior of transparent polyurethane under these conditions is not fully understood. In this study, systematical experiments were performed on transparent polyurethane. The viscoelasticity of the material was firstly verified by several quasi-static cyclic tests. Then a series of large tensile deformation and tensile failure experiments were conducted under various strain rates using a servo-hydraulic high-speed tensile machine. All strain data were acquired by the Digital Image Correlation (DIC) technique. The experimental results show that tensile stress-strain curves and failure behaviors are significantly temperature and strain rate dependent. Finally, a phenomenological-based finite strain viscoelastic model is developed. After parameter identifications, one-dimensional equations are fitted to experimental data that yield good predictions.

***Key Words:*** *Transparent polyurethane; Temperature dependence; Strain rate dependence*

## Introduction

Bird strikes are fatal accidents threatening the safety of aeronautical structures and flight crews, and cause annual commercial loss of $193 million merely in US [1]. A measure to minimize the damage of bird strike is to employ laminated glass as a windshield, which consists of two panes of glass bonded by a polymer interlayer in the simplest case. The interlayer plays a key role on diverse attributes of the windshield, such as transparency, sound attenuation, and mitigation of post-fracture glass fallout. One favourable choice is transparent polyurethane. Polyurethane is a segregated by soft and hard segments. The transparent polyurethane discussed in this paper possesses well elasticity with large deformation capacity, well viscosity with large hysteretic loop, strong impact resistance, low glass transition temperature, firm adhesion, sufficient light transmittance, and so forth. These excellent properties contribute to more extensive applications of transparent polyurethane than many conventional interlayer materials. Structural design is an effective mean to exploit the advantages of laminated glass to the full, which bases on a thorough understanding of involved material such as polyurethane. Under impact loading such as bird strike, the material is in certain conditions. For example, according to experimental results from [1], the speeds of bird strike on aircraft generally ranged from 70 m/s to 250 m/s, which results in strain rate of $10^0$ /s to $10^1$ /s loaded on the structure. Under a blast loading, the interlayer material of laminated glass was at strain rates from 30 /s to 100 /s. Similar to many polymers, polyurethane shows strong strain rate and temperature sensitivity. Taking these factors into account, investigations on large tensile deformation of transparent polyurethane at various intermediate strain rates and temperatures are essential.


Figure 1: Zwick/Roell HTM-2512 servo-hydraulic tensile machine and a high speed camera.

**Experimental study**

In this study, S-123 transparent polyurethane provided by the company PPG was investigated. The material was based on dicyclohexylmethylmethane-4,4-diisocyanate (HMDI), and polytetramethylene ether glycol (PTEG). The light transmittance was over 90% and the density was $1180\ \mathrm{kg{\cdot}m^{-3}}$. Our specimens were designed in flat dumbbell shape in case they broke in the grippers. The specimen had a 10 mm longer gauge section and a 10 mm fillet radius of the arc section. It was 3 mm in thickness and 6 mm in width. Quasi-static tensile experiments were conducted on an Instron 5567 universal testing machine. Note that in quasi-static tests, the low strain rate loading induced more compliant behavior of the specimens than in dynamic tests. As a consequence, the specimens were hard to be gripped tightly. To tackle this problem, specimens were bonded to aluminum shims with glue before being mounted to the grippers. In this study, the tensile experiments at various strain rates were performed on a Zwick/Roell HTM-2512 servo-hydraulic dynamic tensile machine as shown in Fig 1. The tensile force is measured by the inbuilt piezo-electric load cell in the crosshead. There is an embedded transducer to measure the displacement of the gripper. Thanks to the hydraulic system, the test machine can maintain constant stretching speeds available from 0.03 m/s to 12 m/s. The speeds covered the corresponding strain rates from $10^0$ /s to $10^2$ /s.

**Constitutive modelling**

The key ingredient of finite strain based constitutive modelling for polymeric materials is a strain energy function, which can be decomposed as an isochoric contribution and a volumetric as

$$\Psi(\boldsymbol{C},\boldsymbol{A}) = \tilde{\Psi}_{vol}(J) + \tilde{\Psi}_{iso}(\bar{\boldsymbol{C}},\boldsymbol{A}) = \tilde{\Psi}_{vol}(J) + \tilde{\Psi}^{e}_{iso}(\bar{\boldsymbol{C}}) + \sum_{i=1}^{s} \tilde{\Psi}^{v}_{iso,i}(\bar{\boldsymbol{C}},\boldsymbol{A}_i) \tag{1}$$

where $J = \det\boldsymbol{F}$, $\bar{\boldsymbol{C}} = J^{-2/3}\boldsymbol{C}$ and $\boldsymbol{A}$ is an internal variable . Similar to the decoupled representation of the energy function, the corresponding decoupling of the stress tensor yields

$$\boldsymbol{S} = \boldsymbol{S}_{vol} + \boldsymbol{S}_{iso} = 2\frac{\partial\Psi_{vol}}{\partial\boldsymbol{C}} + 2\frac{\partial\Psi_{iso}}{\partial\boldsymbol{C}}. \tag{2}$$

In Eqn. (2), we have $\boldsymbol{S}_{vol} = Jp\,\boldsymbol{C}^{-1}$, where the hydrostatic pressure $p = \partial\Psi_{vol}(J)/\partial J$ has been introduced. In the case of incompressibility, $J = 1$ and $p$ serves as a Lagrange multiplier

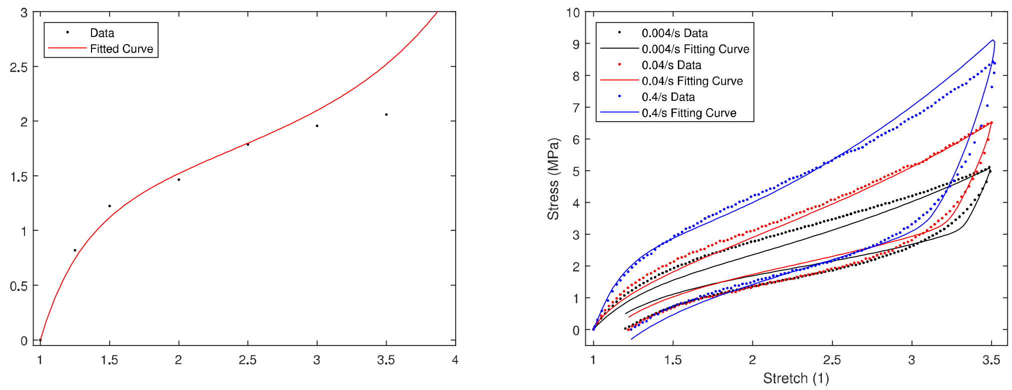


Figure 2: A complete set of material parameter identification using (Left) Elastic data, (Right) Viscoelastic data at various strain rates of 250% deformation

to satisfy this kinematic constraint on the deformation field. The isochoric energy function $\Psi_{iso}$ is expressed in terms of the isochoric right Cauchy-Green tensor $\bar{\boldsymbol{C}} = \bar{\boldsymbol{F}}^t \bar{\boldsymbol{F}}$, $\bar{\boldsymbol{F}} = J^{-1/3}\boldsymbol{F}$. The definition of the stress tensor $\bar{\boldsymbol{S}} = 2\partial\Psi_{iso}(\bar{\boldsymbol{C}}, \boldsymbol{A})/\partial\bar{\boldsymbol{C}}$ is introduced and the isochoric stress $\boldsymbol{S}_{iso}$ is related to the previous one via the fourth-order projection tensor $\mathbb{P} = \partial\bar{\boldsymbol{C}}/\partial\boldsymbol{C}$ by

$$\boldsymbol{S}_{iso} = J^{-\frac{2}{3}}\mathbb{P} : \bar{\boldsymbol{S}} \qquad \text{with} \qquad \mathbb{P} = \mathbb{I} - \frac{1}{3}\boldsymbol{C}^{-1} \otimes \boldsymbol{C} \quad , \quad \mathbb{I}_{ijkl} = \delta_{ik}\delta_{jl} \tag{3}$$

where $\delta_{ij}$ is a Kronecker delta. The stress $\bar{\boldsymbol{S}}$ is further decomposed into elastic and viscous parts, i.e. $\bar{\boldsymbol{S}} = \bar{\boldsymbol{S}}^e + \bar{\boldsymbol{S}}^v$. A Carrol type elastic energy is chosen as

$$\Psi^e_{iso}(\bar{\boldsymbol{C}}) = aI_1 + b\bar{I}_1^4 + c\sqrt{\bar{I}_2} \tag{4}$$

where $a, b, c$ are material parameters. Lubliner [3] proposed a viscous energy function as

$$\Psi^v_{iso} = \sum_{i=1}^{s} \frac{1}{2}\mu_i^v \left[ (\boldsymbol{A}_i : \bar{\boldsymbol{C}} - 3) - \ln\det(\boldsymbol{A}_i) \right] \tag{5}$$

where $\mu_i^v$ is a viscous shear modulus and $\boldsymbol{A}_i$ are the strain-like tensorial variables associated with viscous Maxwell elements. A thermodynamically consistent evolution ansatz for the internal variable of a single element follows

$$\dot{\boldsymbol{A}}_i = \frac{1}{\tau_i}\left[ \bar{\boldsymbol{C}}^{-1} - \boldsymbol{A}_i \right], \tag{6}$$

where $\tau_i$ is the relaxation time. All of the tests presented in the previous section are of uniaxial type. Therefore, the constitutive model discussed above needs to be formulated in one-dimensional form in order to identify the material parameters as well as to validate the model. From the incompressibility condition, i. e. $\det\boldsymbol{F} = \det\bar{\boldsymbol{F}} = \lambda_1\lambda_2\lambda_3 = 1$ and the assumption of symmetry the complementary principal stretches follow as $\lambda_2 = \lambda_3 = \lambda^{-1/2}$. Therefore, the complete deformation gradient reads $\boldsymbol{F} = \left[\lambda, \lambda^{-1/2}, \lambda^{-1/2}\right]$. The total stress can be obtained as

$$P \;=\; \left[2a + 8b[2\lambda^{-1} + \lambda^2]^3 + c[1 + 2\lambda^3]^{-\frac{1}{2}}\right] [\lambda - \lambda^{-2}] + \sum_{i=1}^{s} \mu_i^v \left[ \lambda\lambda_i^{2,A} - \frac{1}{\lambda^2\lambda_i^A} \right], \tag{7}$$

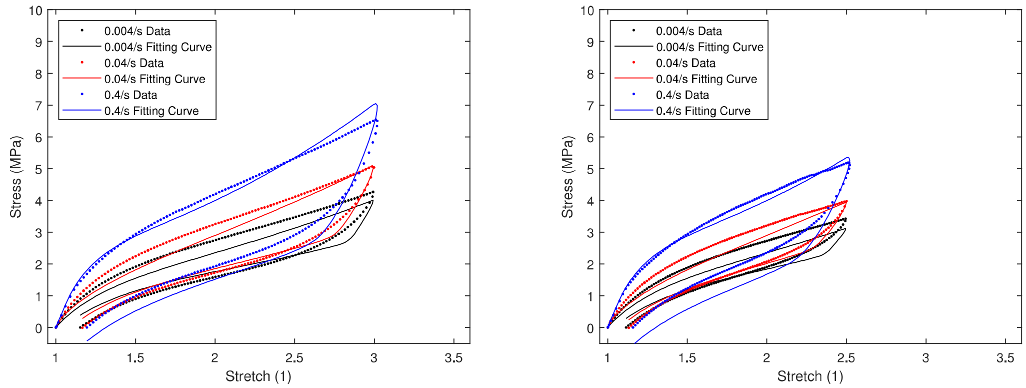


Figure 3: Model validation with other strains (Left) $200\%$ deformation, (Right) $150\%$ deformation

Table 1: Identified elastic and viscoelastic material parameters, respectively; $\mu$, $\mu_i^v$ in [MPa] and $\tau_i$ in [s]

| a | b | c | $\mu_1^v$ | $\mu_2^v$ | $\mu_3^v$ | $\mu_4^v$ |
|---|---|---|---|---|---|---|
| 2.29e-01 | 5.93e-06 | 1.67 | 2.68e-1 | 1.4 | 9.71e-2 | 8.14e-2 |
| - | - | - | $\tau_1$ | $\tau_2$ | $\tau_3$ | $\tau_4$ |
| - | - | - | 1.36e-3 | 1.88 | 3.63e2 | 5.36e4 |

Similar to the one-dimensional formulation of the total stress, the evolution law is derived:

$$\dot{\overline{\lambda_i^{2,A}}} = \frac{1}{\tau_i}\left[\lambda^{-2} - \lambda_i^{2,A}\right]. \tag{8}$$

Now a parameter identification algorithm is used to find a complete set of parameters of the model in Eqn 7. At first, the elastic part of the equation is used to identify parameters $a, b, c$. Elastic parameter fitting is shown in Fig 2(left). Afterwards, another set of data is incorporated to identify viscous parameters $\mu_i, \tau_i$, see Fig 2(right). During the viscous parameter identification, the elastic parameters are kept frozen. A complete set of identified parameters is presented in Table 1. With the identified parameters, other set of data are compared with the model to find model validation which find good agreements, see Fig 3.

**Conclusions**

In this study, a comprehensive experimental study was conducted to characterise viscoelastic behaviours of a widely used polymeric material, i.e., Transparent Polyurethane. After that, a large strain-based material model is proposed which predicts many data that are not included in the parameter identification process.

**References**

1 Liao Z S, Yao X H, Zhang L H, Hossain M, Wang J, Zang S. *International Journal of Impact Engineering* , 129:152-167, 2019.

2 Linder C, Tkachuk M, Miehe C, *Journal of the Mechanics and Physics of Solids*, 59:2134-2156, 2011

3 Hossain M, Vu D K, Steinmann P, *Computational Materials Science*, 59:65-74, 2012